A complex subglacial water system below the South Pole of Mars unveiled by new MARSIS data

Lauro S.E.[1], Pettinelli E.[1]*, Caprarelli G.[2], Guallini L.[1], Rossi A.P.[3], Mattei E.[1], Cosciotti B.[1], Cicchetti A.[4], Soldovieri F.[5], Cartacci M.[4], Di Paolo F.[1], Noschese R.[5], and Orosei R.[6]

Affiliations:

1 Dipartimento di Matematica e Fisica, Università degli studi Roma Tre, Rome, Italy

2 School of Sciences, University of Southern Queensland, Toowomba, Australia

3 Department of Physics and Earth Sciences, Jacobs University Bremen, Bremen, Germany

4 Istituto di Astrofisica e Planetologia Spaziali (IAPS), Istituto Nazionale di Astrofisica (INAF), Rome, Italy

5 Istituto per il Rilevamento Elettromagnetico dell'Ambiente, Consiglio Nazionale delle Ricerche, Naples, Italy

6 Istituto di Radioastronomia (IRA), Istituto Nazionale di Astrofisica (INAF), Bologna, Italy

Corresponding author: pettinelli@fis.uniroma3.it

Abstract

The recent detection of a body of liquid water at the base of the Martian South Polar Layered Deposits (SPLD) by the Mars Radar for Subsurface and Ionospheric Sounding (MARSIS) has reinvigorated the debate about the origin and stability of liquid water under present-day Martian conditions. To further explore the study area (Ultima Scopuli) and investigate the possible nature and extent of the water, we acquired new radar data to provide a denser coverage of the area relative to the earlier study. We analysed the complete MARSIS dataset acquired over the region using signal processing procedures commonly applied on Earth to discriminate between wet and dry subglacial areas. The results of this new study independently corroborate the previous detection of a significant basal body of liquid water at the base of Ultima Scopuli and provide evidence for other wet areas in its surroundings, suggesting a complex hydrologic network deserving of further investigation. Here we also suggest that the subglacial water is likely to be hypersaline perchlorate brines, which are known to form at the

polar regions of Mars and have been shown to survive for geologically significant periods of time at temperatures far below their eutectic values.

Orbiting subsurface radar sounders are powerful geophysical tools to investigate a planetary crust at shallow depths. This technique employs a burst of radio waves to image the buried geological structures in a similar fashion to active seismic prospection. As radio waves propagate with little attenuation in ice, this method is particularly well suited to study the internal structure of the Martian Polar Layer Deposits (PLDs)[1] and to detect the bedrock below such deposits[2]. The possible identification of subsurface liquid water was one of the main goals to develop MARSIS (Mars Advanced Radar for Subsurface and Ionosphere Sounding), a radar sounder similar to those used on Earth to search for subglacial water[3]. The sounder was launched in 2003 onboard the Mars Express spacecraft and began to collect data in the summer of 2005. After several years of data acquisition, however, the lack of any clear evidence of basal liquid water below the Martian Polar Caps started to challenge the original hypothesis[4], suggesting that water, if present, may be located at a greater depth than previously thought[5,6]. The recent radar detection by Orosei et al.[7] of subglacial liquid water in Ultima Scopuli, at the base of the South Polar Layered Deposits (SPLDs), reignited the scientific debate about present-day stability of liquid water at the Martian poles. The discovery was based on the analysis of 29 radar profiles collected by MARSIS over a 200x200 km^2 area centered at 193°E 81°S, with the ratio between basal and surface echo intensity highlighting two distinct areas, one bright and one non-bright. Using a robust probabilistic approach[8] two different probability density functions of the basal permittivity were retrieved, from which wet (bright) and dry (not-bright) basal conditions were determined. Because the nature of the body of liquid water detected by MARSIS was not addressed in detail in Orosei et al.'s paper[7], in the present work we extend our investigation to constrain and define the characteristics and spatial distribution of the subglacial bright areas associated with basal liquid water and we discuss possible physical and chemical conditions to explain formation and persistence of such water at the Martian south polar regions. We increased the area coverage with 105 new MARSIS observations and applied a methodological approach adapted from signal processing procedures commonly used in terrestrial radar sounding to discriminate between wet and dry sub-glacial basal conditions. This approach strongly improves our capability to identify water body candidates and test the reliability of their detection, enabling us to localize the position and extent of several subglacial bodies of liquid water, in addition to that found by Orosei et al.[7]. These findings confirm Orosei et al.'s[7] discovery, and further highlight a complex hydrology for the SPLDs at Ultima Scopuli.

Presently Mars is a cold hyper-arid desert, but it may not have always been so. The geological record clearly demonstrates that the climate has undergone dramatic changes throughout Mars's planetary history, even though our understanding of the processes responsible for such evidence is still incomplete. Geological, morphological and compositional data from Late Noachian to Early Hesperian (~3.7 Ga) terrains[9-14] indicate the past existence of warm and wet periods characterized by temperatures above the freezing point of water, abundant rainfall, and fluvial processes on the surface of Mars. Recently, however, Palumbo et al.[15] and Palumbo and Head [16] have argued that climate models fail to produce global Martian warm and wet periods, and that precipitation was mostly in the form of snow rather than rain. If this is true, direct surface runoff could not have produced a significant morphological signature on the Martian surface. They alternatively proposed that the observed "wet" morphologies on Mars were formed through snow accumulation, snow melting and the resulting secondary runoff**.**

The transfer of water between the Martian cryolithospheric and atmospheric global reservoirs is linked to the variability of orbital parameters[17], with it being generally accepted that quasi-periodic variations of orbital eccentricity[18] and planetary obliquity[19-22] had profound effects on the Martian climate[23]. Proof of the effects of orbital forcing on the climate of Mars is evident in the stratigraphy of the north polar layered deposits (NPLDs), for which there is good correspondence between the timescales of layer deposition and astronomical cycles[21]. The relationship between orbital parameters and the origin, timing and evolution of the layered deposits at the south pole is however still largely unconstrained and problematic[24,25], and many more data are needed on the composition and physical properties of the SPLDs to understand the mechanisms for their formation and evolution. It is therefore especially critical to continue expanding the dataset, performing new processing, and broadening the search area started by Orosei et al[7]. Under present-day climate conditions, the Martian polar caps are generally assumed to be cold-based[1]. However, the Late Noachian-Early Hesperian circumpolar Dorsa Argentea Formation displays characteristic esker-like morphologies that have been interpreted as evidence of basal melting under thick ice sheets[26], likely made possible by a combination of warmer and wetter climate conditions[27] and a significantly higher heat flux (~ 45-60 mW/m^2) than at present (20-22 mW/m^2)[28]. Furthermore, ice-sheet structures and km-scale tectonic deformations in the Late Amazonian SPLDs[29,30] provide evidence of broad ice movement, suggesting localized basal melting of the Martian southern ice sheet under possible warmer conditions[31].

The set of physical conditions conducive to basal melting at the Martian polar and subpolar regions has been explored by some authors[31-33] via the theoretical combination of heat flow parameters that could result in ice melting at the base of the south polar ice cap. Recently Sori and Bramson[34] suggested that a high geothermal gradient (heat flux $\geq$72 mW/m^2) is needed for basal melting of the SPLDs, regardless of the salinity level. The same authors thus postulated that magmatic activity must have occurred in the region less than a million years ago for a liquid water body to exist at the base of the SPLDs. Evidence for late Amazonian (as young as 2 Ma) magmatic activity has been reported in the Elysium region[35,36], suggesting the potential for localized high geothermal gradients on Mars in recent geological times. An anomalously high geothermal gradient is, however, not the only possible cause for temperature increases at the base of extensive ice-sheets. For example, localized basal melting of a thick Early Amazonian polythermal ice sheet in Isidis Planitia was modeled by Souček et al.[37], who concluded that subglacial wet areas could form under climatic and geologic conditions that are not significantly different from those on present-day Mars.

Terrestrial analog studies also indicate that subglacial water reservoirs are common in topographic troughs bound by tectonic structures[38,39]. Previous radar sounder investigations of the basal interface between the SPLDs and bedrock have found irregular morphologies, characterized by plains, topographic highs and basins at very high latitudes[40] potentially favorable for the flow and trapping of fluids under the SPLDs. Conversely, the basal topography in the investigated region does not show any appreciable depression (Methods).

Radar detection of Martian subglacial water: A lesson from the terrestrial ice-caps

On Earth, Radio-Echo Sounding (RES) represents one of the most valuable methods to detect subglacial bodies of liquid water[3]. This technique is able to image the internal structure of an ice sheet from surface to bedrock[41]. The combination of qualitative (bedrock morphology in the radar image) and quantitative (signal features) analysis leads to the detection of the subglacial water. Historically, four specific criteria have been proposed to identify and categorize the subglacial lakes in East Antarctica[42]: i) standard deviation of the echo strength (values lower than 3dB indicate that the basal interface is smooth at the scale of the radar footprint); ii) high echo strength relative to the immediate surroundings; iii) absolute echo strength (related to the basal reflection coefficient); and iv) the assumption that a subglacial lake is hydraulically flat[43,42]. According to such criteria East Antarctic subglacial lakes have been classified as: *definite lakes*, at least partially satisfying all four criteria; *dim lakes*, which satisfy the first two quantitative criteria; *fuzzy lakes*, which only satisfy the absolute and relative signal intensity requirements; *indistinct lakes*, characterized by low standard deviation in echo intensity; and *failing lakes*, that only satisfy one of the four criteria[42]. Recently these criteria have been partially modified and updated to identify more complex subglacial water distribution (e.g., active lakes) [44] by using the specularity content related to the angular distribution of the basal scattering[45,46]. In Greenland, given the paucity of subglacial lakes[47], RES data have been mainly used to constrain the subglacial basal conditions and to define the spatial distribution of the water (ponded/thawed/frozen) at the ice-sheet bed, mainly using the “pulse peakiness” of the bed echo signal (abruptness or acuity)[48-52] and the bed echo intensity variability[53]. Recently, however, several previously undetected subglacial lakes have been found by applying some of the criteria originally used in East Antarctica[54]. Some of these criteria, together with the specularity content, have also been applied to RES data collected in the Canadian Arctic, resulting in the discovery of the first two isolated hypersaline subglacial lakes on Earth[55].

MARSIS radar is, in principle, very similar to the systems used in RES investigations, although several aspects limit the number of criteria that can be applied to detect the basal water below the Martian polar caps. Given the operating frequency (1.8-5 MHz), the antenna dimension (40 m) and the altitude of the spacecraft (250-900 km), MARSIS pulse limited radius footprint is very large (from 6 to 11 km) compared to footprints of the common RES radar allocated on airborne platforms and working at higher frequencies (typically of the order of 100m). The bright area below the SPLDs interpreted as a stable body of liquid water[7] was estimated to be approximately 20 km in extent, i.e., comparable to the dimension of the MARSIS pulse limited footprint. The vertical (~55m in ice) and horizontal (~7km) resolution of MARSIS (Methods) prevents a detailed characterization of the bedrock morphology, topography and hydraulic potential, as the uncertainties associated with the estimation of such parameters are similar in magnitude to the range of measured variations (Supplementary Fig.2). Moreover, as the MARSIS antenna could not be calibrated[56] and the signal absorption in the SPLDs is not well constrained, the basal reflection coefficient (absolute echo strength) criterion cannot be applied. Given these technical limitations the approach used here to analyze MARSIS data mainly follows the methodology tested in Greenland to discriminate between ponded water and frozen or dry basal conditions. Such a methodological approach is based on signal intensity (which is an indication of the basal reflectivity), signal acuity (which is associated with the smoothness of the bed[52]) and bed-echo intensity variability (which detects the transition from dry to wet materials at the base of the ice[53]) (Methods). Note that each parameter has been computed for both surface and basal echoes and then normalized to the median of the relevant surface parameter in order to minimize the effects caused by local surface echo power fluctuations, which are sometimes observed in the data, without altering the along track variation of the basal reflectivity and acuity (Methods).

New MARSIS data analysis

The analysis presented in this work was performed on the data acquired in 134 radar profiles during multiple campaigns over Ultima Scopuli from 2010 to 2019 (Figure 1a). We focused on a

250x300 km^2 zone (blue box in Figure 1a), around and including the bright area previously identified by Orosei et al.[7], where we have significant data coverage (90 observations) and many radar profiles that cross each other (Figure 1b). Given the MARSIS pulse length of about 200 m in air, the surface of the studied area can be considered smooth with elevation gently decreasing northward (Figure 1a). The basal interface (bottom of the SPLDs) is clearly detectable in all radar profiles and it is thus possible to estimate the local thickness of the SPLDs under the assumption that the signal velocity does not change in the entire investigated area. Immediately around the bright area the thickness of the SPLDs is constant (considering the pulse length and the footprint) but at the regional scale it progressively decreases in the same direction as the surface (see Figure 2), resulting in an essentially flat basal topography (Supplementary Fig.2). We acquired data at three MARSIS frequencies: 3, 4 and 5 MHz. The 4MHz dataset was the most complete, and therefore we applied our analysis to this specific dataset in order to improve the robustness of our statistical analysis. Even if not further discussed here, we note that the 3 and 5 MHz data and their processing results are consistent with those obtained from the 4 MHz dataset (Supplementary Fig.1).

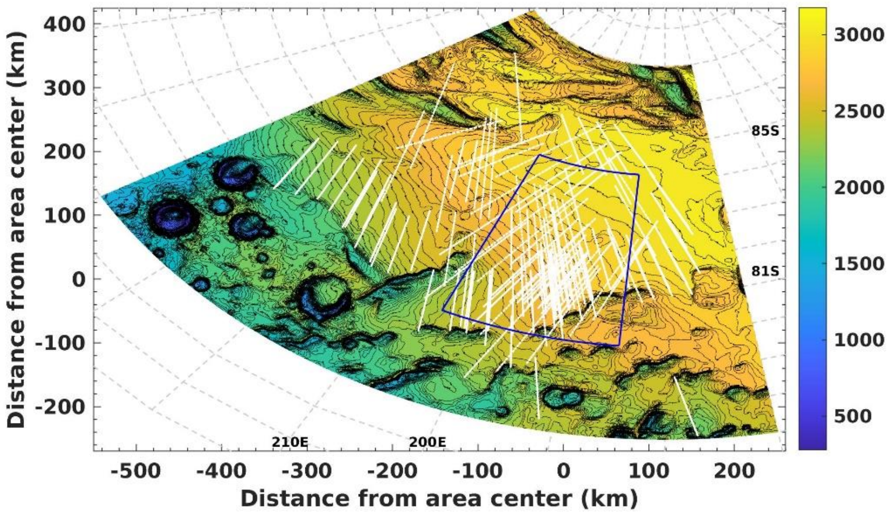

(a)

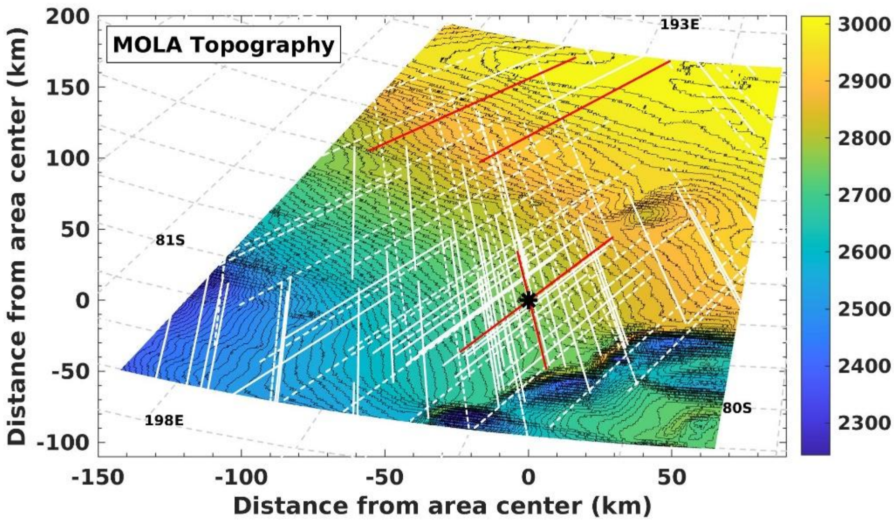

(b)

Fig. 1 (a) Ultima Scopuli Mola topographic map and location of MARSIS radar profiles collected in the region. Solid white lines are Super-frame data and dash white lines are Flash memory data (Methods). Blue box delimits the investigated area. (b) Detail of the investigated area (the blue box in Fig. 1a). Red lines (observation number 12854, 12861, 10737, 14853) highlight the radar profiles used to describe the three diagnostic parameters (Fig.3) that were applied to discriminate between wet and dry areas. The black star indicates the center of the bright area detected by Orosei et al. [7] at 193°E and 81°S.

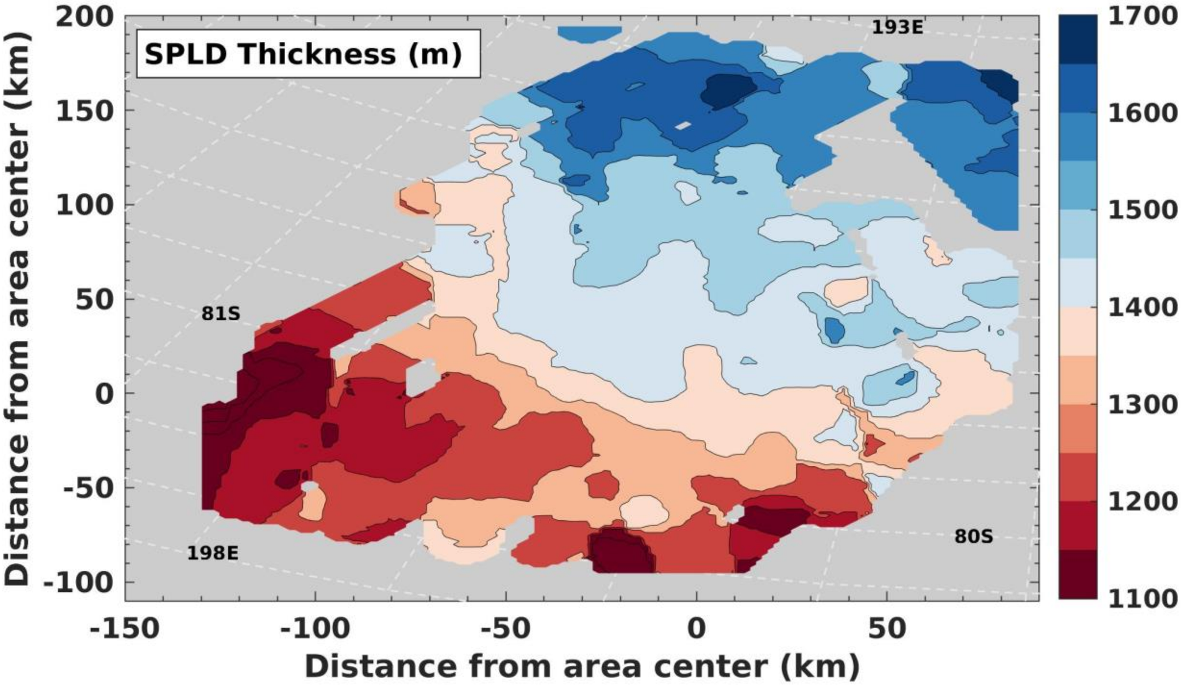

Fig. 2 SPLD thickness computed assuming a velocity value of 163 m/μs (ε_{ice}=3.4). Gray areas indicate no data available.

In order to describe the meaning of the three chosen diagnostic parameters (intensity, acuity and bed-echo intensity variability) in terms of basal water detection, we selected four representative radar profiles in the investigated region (red lines in Fig. 1b): two outside (observations 12854 and 12861) and two across (observations 10737 and 14853) the previously detected bright area . We analyzed the trend of these parameters along the observations and compared the spatial behavior of each parameter between observations (see Fig. 3). The surface values of intensity and acuity (black lines in Fig. 3) are broadly similar in both areas, with limited variations along each observation indicating a smooth and flat surface at the MARSIS wavelength. Conversely, the basal values (red lines in plots of Fig. 3) are markedly different. In the background area, along orbits 12854 and 12861, basal intensity and acuity values are constant and much lower than the corresponding surface values, whereas the intensity variability is always above the surface values. These parameters suggest a low reflectivity of the basal material (-10 dB relative to the surface), a relatively rough basal interface (low acuity) and a spatially homogeneous bedrock (relatively constant intensity variability along tracks).

Conversely, the observations acquired across the bright area show a marked increase of the basal intensity (about 10 dB) along track, reaching a maximum value (well above the surface values) at the center of the bright area. Similar trends are observed in the basal acuity values, while intensity variability values change abruptly where the observations approach the bright area. According to Oswald et al.[52], the occurrence of high intensity and high acuity values in the same location indicates the presence of ponded water, and Jordan et al. [53] have shown that intensity variability values exceeding 6 dB mark the transition (edge detector) between dry and wet materials. Moreover, Dowdeswell and Siegert[57] emphasized that a change in basal intensity of about 10 dB along track could be evidence of the presence of a lake, whereas smaller variations (e.g., on the order of 2dB) could indicate wet sediments or water intruded in the bedrock around a lake[42]. The combination of the three criteria makes the interpretation of the basal conditions along the four profiles quite robust and suggests a remarkable difference in the bed material properties between the two areas: observations 12854, 12861 detected a dry (or frozen) bedrock, whereas observations 10737, 14853 crossed at least one large water ponded area.

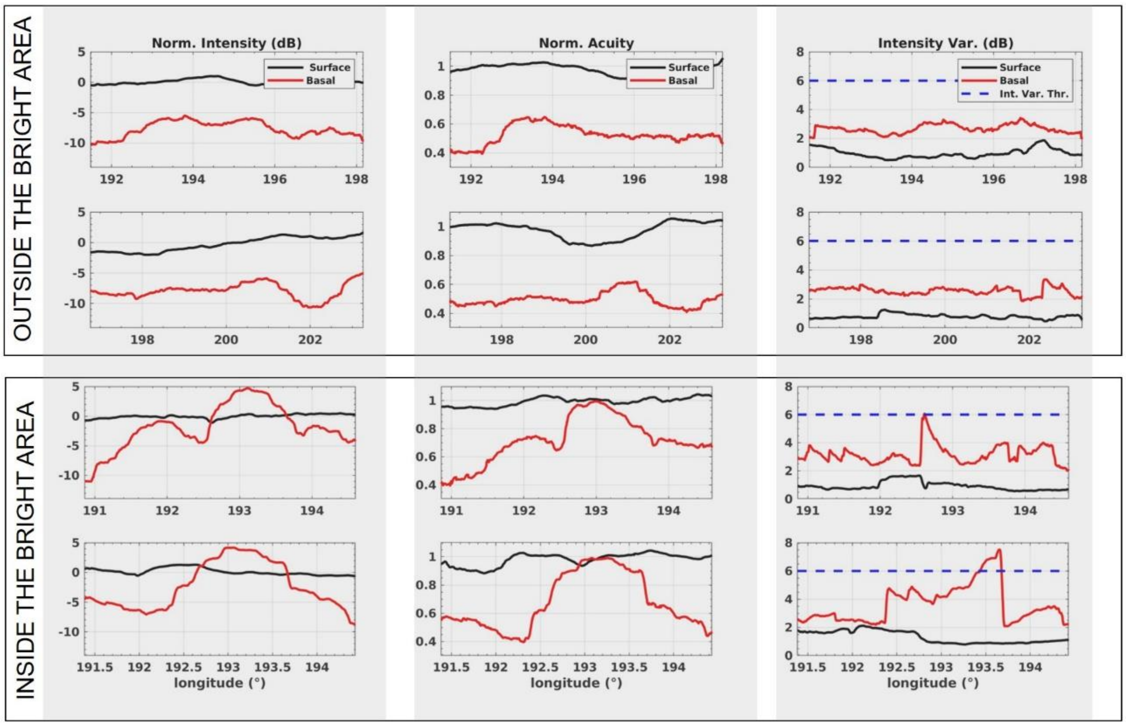

Fig. 3 Data collected outside and inside the bright area. From top to bottom observations are: 12854, 12861, 10737, 14853. Black lines indicate surface and red lines basal parameters. In the right column the dash blue line indicates the water detection threshold (6 dB) according to Jordan et al.[53].

To assess the wet/dry spatial distribution of the basal material below the SPLDs, we used all observations collected in the study area (Fig. 1b) and generated a basal intensity map and a basal acuity map (Fig. 4). Both maps clearly show two distinct areas: an upper southern area characterized by a very low and relatively constant signal intensity [from -14 to -6 dB] and acuity [from 0.3 to 0.6] and a lower northern area characterized by several patches of high signal intensity [from -3 to 4 dB] and acuity [from 0.65 to 1]. Comparison of the two maps (Fig. 4) highlights the strong spatial correlation between the two parameters with only few exceptions, where high values of basal acuity do not correspond to high values of basal intensity and vice versa. Therefore, following Oswald et al.[52], we conclude that the basal material in the southern area is uniformly dry whereas the northern area is characterized by the presence of several basal patches of ponded water.

These results corroborate the initial discovery by Orosei et al.[7] of a stable body of liquid water in Ultima Scopuli using a different and independent technique, while at the same time highlighting a more extensive, complex situation with ubiquitous water patches surrounding the subglacial lake. This is illustrated through the correlation of the features mapped in Fig. 4 and the plots of the radar parameters of orbit 10737 (third row in Fig. 3). The trend of basal intensity and acuity in the plots shows that the ponded area centered at 193°E-81°S (point 0,0 in the maps) is surrounded by other, weakly spatially constrained wet areas whose distribution is reminiscent of a fuzzy lake, typically characterized by a large body of water encircled by patchy water pools or wet areas of smaller extent[42]. This interpretation is also supported by the intensity variability values computed on other observations partially crossing the lateral water patches (Supplementary Fig.4 and Fig.5). The abrupt transitions in bed material properties are still well detectable, however the variability values at the edge of the patches are slightly lower than the 6dB threshold[53], probably due to the fact that the patches are not completely intercepted by the radar footprint and/or that they consist of wet sediments or small volumes of water (Supplementary Fig.3).

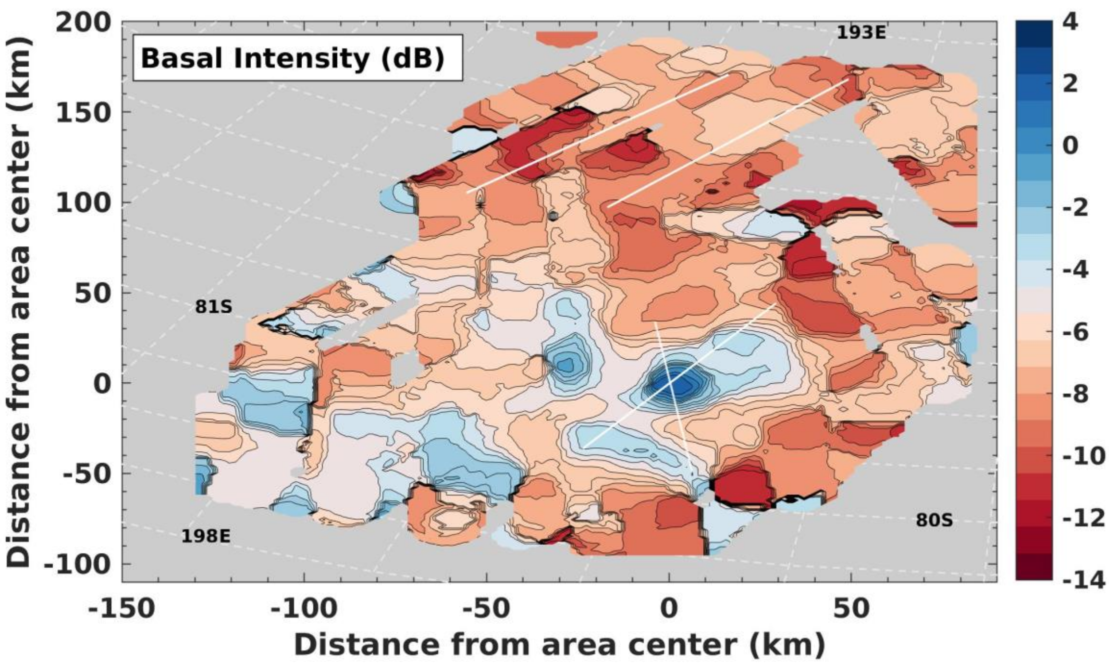

(a)

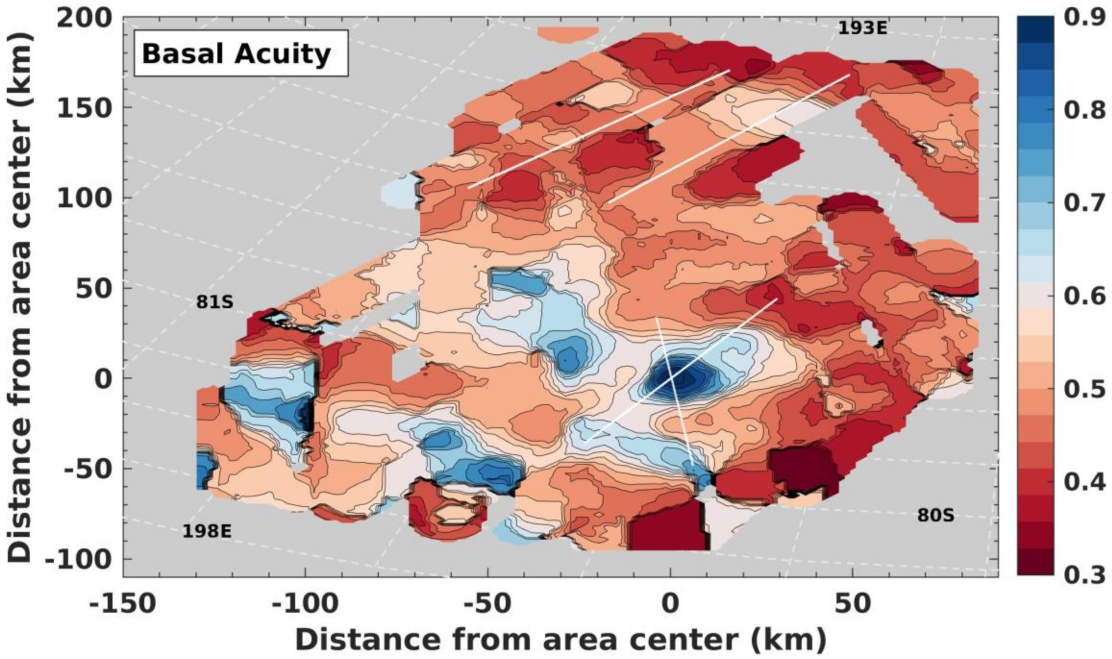

(b)

Fig. 4 Spatial distribution of the normalized basal reflectivity (a) and normalized basal acuity (b) computed from the radar data collected at 4 MHz. White lines highlight the same red lines (observations) shown in Fig. 1b and used for the analysis of Fig. 3.

As a final step, we extended the approach followed by Orosei et al.[7] to compute the basal water distribution map in terms of permittivity (Fig.5), in the area where a significant number of samples were present (Supplementary Fig. 6) and where the radar profiles were crossing each other (Methods). The map shows that the areas with high values of basal permittivity (15-40) correspond to the smooth areas (high acuity values) shown in Fig.4b, whereas the surroundings exhibit much lower values (about 6-8). On Earth, a permittivity value of 15 can be considered to be a threshold for the presence of liquid water in the basal material[7]; values below such threshold indicate that the material is dry or frozen. It is interesting to note that the central pond (permittivity ~40), which corresponds to the original main body of liquid water detected in Orosei et al.[7], is separated from the other pools by strips of dry basal material. It is also the widest body of water and probably has the largest volume of liquid water of the entire hydraulic network.

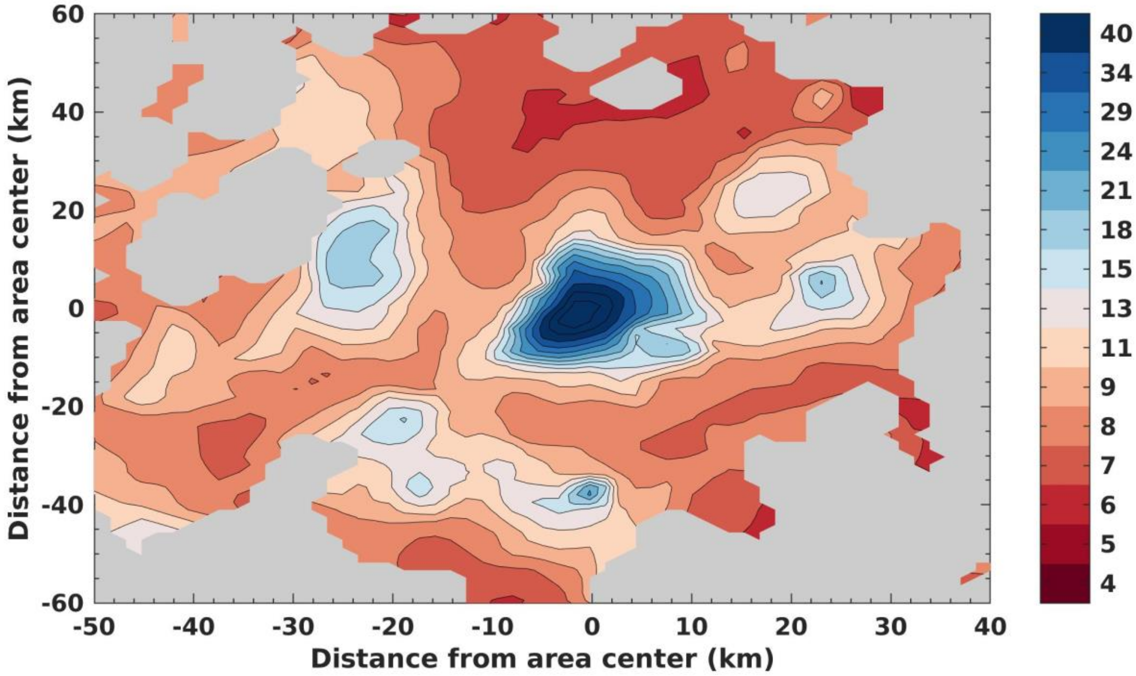

Fig. 5 Relative dielectric permittivity map computed by inverting the radar data. The gray patches correspond to areas where the number of samples is lower than 100, which is the minimum threshold to apply the probabilistic approach. This procedure has reduced the dimension of the study area to 90x120 km^2.

Mars subglacial lakes and the possible role of brines

Terrestrial subglacial lakes are known to have a variety of origins. Some are the remnants of isolated subaerial water bodies subsequently covered by ice sheets, as shown in the Canadian Arctic[58,55] and in Antarctica[59,60], while others are hydrologically linked in a system of aquifers recharged by surface melting[47] or by ocean waters[61]. Investigations of the subglacial lakes of Antarctica[62-64] highlight the critical contribution of the regional geological history to the formation and persistence of standing bodies of liquid water. Endogenic processes concurred to both the formation of topographic lows into which liquid water could flow and the existence of high geothermal gradients[65-68,54], as attested by the presence of volcanoes active in the Holocene (no earlier than ~ 12,000 years ago). Complex thaw-freeze cycles at the boundaries of the lakes, related to ice accumulation rates, and ice flow dynamics play a major role in the history of lake recharge and water residence times[69].

The technical and spatial resolution limitations of the MARSIS dataset do not allow a direct comparison of these Earth analogs with the Martian case. Furthermore, the unique combination of physical, geological, climatic and topographic conditions that could favor the formation of liquid water and its long term survival in a subglacial lake at the base of the SPLDs is, at best, a matter of speculation at this point in time. It is, however, possible to interpret relevant observations in the context of known experimental data and terrestrial analog studies to propose plausible processes for the formation and persistence of subglacial liquid water on Mars. Combining evidence from radar datasets and thermal models, subglacial hypersaline aqueous solutions were found to persist on Earth at temperatures much lower than the freezing point of water[70]. Thus, brines have been proposed as the most plausible form of liquid water on the Martian surface and subsurface under present-day physical conditions[71], and have indeed been observed to flow on the Martian surface[72].

The process of absorption of atmospheric water by perchlorates and the subsequent formation of hypersaline solutions (i.e., deliquescence) was directly observed at the Phoenix Landing Site[73]. Considering that Ca-, Mg-, Na- and K- perchlorates, chlorates and hydrated chlorides[74-77] are globally ubiquitous in the Martian regolith, we posit that deliquescence and the formation of brines plausibly occurs at the south polar latitudes as well. Experimental work has shown that soluble salts with low eutectic temperatures deliquesce at low relative humidity values over a wide range of temperatures, overlapping with those expected on Mars[78-80], suggesting that brines may readily form in sub-polar regions when the temperatures are in the higher range (e.g., at noon). Re-crystallization of brines (efflorescence) when temperatures drop, however, is often kinetically inhibited[81] because high activation energies are required for the transition from liquid to solid (ordered) states. Freezing experiments conducted under conditions similar to those on Mars have shown that perchlorate and chloride brines may exist for long times after their formation without efflorescing[82,83]. It is therefore plausible that once formed, brines may exist on Mars in a metastable state for geologically significant periods of time[84].

Orosei et al.[7] suggested that the subglacial water discovered at Ultima Scopuli could be hypersaline solutions. Subsequently, Sori and Bramson [34] computed the geothermal flux at the base of the SPLDs that would melt ice when Na-, Mg- and Ca- perchlorates are present in the icy mixture. They used Pestova et al.'s [85] eutectics for Mg- and Ca-perchlorate aqueous solutions, and Chevrier et al.'s[86] eutectics for Na- perchlorate solutions, determining that an anomalously high geothermal flux of 72 mW/m^2 is required for the icy mixture to achieve the temperature of the lowest eutectic (Ca-perchlorate, 199 K). Recent experiments have shown, however, that Mg- and Ca-perchlorate-H_2O solutions remain liquid in a super-cooled state at temperatures as low as 150 K[87]. Mean temperatures at the Ultima Scopuli location have been estimated to be approximately 160 K at the surface[7], increasing with depth by a few to a few tens of K per km, depending on the unknown geothermal flux and thermal properties of the SPLDs. These temperatures are very close to the lower boundary of super-cooled solutions, where kinetic processes are particularly important. We argue therefore, that thermophysical modeling based on equilibrium conditions may not be wholly realistic in this context and propose instead that metastable conditions are likely to produce a geologically significant effect, both in terms of the formation of brines and in terms of their longevity on Mars.

Our new and expanded methodological approach to the analysis of the earlier[7] and new MARSIS data confirms the presence of a water lake at the base of the SPLDs in Ultima Scopuli, and further suggests that the bottom of the SPLDs is characterized by discrete areas of wetness around the main water body, possibly indicating that patches of ponded liquid water are not uncommon. Unfortunately, however, it will be difficult to find such bodies in other areas due to the unique surface characteristics of the investigated area (flat topography and smooth surface) and the limitations of the space-borne radar method. In any case, we are unable to conclusively determine whether the discovered Ultima Scopuli water bodies are hydrologically linked, but we believe that the new evidence presented here will substantially contribute to our understanding of the Martian hydrologic cycle.

Orosei et al.[7] suggested that water at the base of the SPLDs was prevented from freezing owing to a high concentration of dissolved salts. In this paper we have presented a qualitative discussion on the conditions of brine stability which supports that interpretation. In the absence of heat flow data or geological evidence pointing to geothermal anomalies, models advocating recent magmatic activity to explain melting at the base of the SPLDs rely on largely speculative assumptions that disregard other key evidence acquired from planetary observations to date. We do not exclude the possibility that future missions might detect anomalous geothermal gradients in this region of Mars. We argue, however, that known physical and chemical properties of hypersaline aqueous solutions already provide a viable interpretive framework based on current observations and measurements of properties of the Martian surface and subsurface.

The possibility of extended hypersaline water bodies on Mars is particularly exciting because of the potential for the existence of microbial life, such as extremophiles, anaerobes[88] or even aerobes (considering that the solubility of O_2 in brines is up to 6 times the minimum level required for microbial respiration[89]). The water bodies at the base of the SPLDs therefore represent areas of potential astrobiological interest and planetary protection concern, and future missions to Mars should target this region to acquire experimental data in relation to the basal hydrologic system, its chemistry, and traces of astrobiological activity.

Data and materials availability: The code that produces the figures and numerical results stated in the text is available from the corresponding author on reasonable request.

References

1. Phillips RJ et al. Mars north polar deposits: Stratigraphy, age, and geodynamical response. *Science* **320**, 1182-1185 (2008).
2. Picardi, G., Plaut, J. J., Biccari, D., Bombaci, O., Calabrese, D., Cartacci, M., ... & Federico, C. Radar soundings of the subsurface of Mars. *science*, *310*(5756), 1925-1928 (2005).
3. Siegert, M. J. A 60-year international history of Antarctic subglacial lake exploration. *Geological Society*, London, Special Publications, **461**(1), 7-21(2018).
4. Clifford, S. M. A model for the hydrologic and climatic behavior of water on Mars. *Journal of Geophysical Research*: *Planets* **98**.E6: 10973-11016 (1993).
5. Clifford, S. M., Lasue, J., Heggy, E., Boisson, J., McGovern, P., & Max, M. D. Depth of the Martian cryosphere: Revised estimates and implications for the existence and detection of subpermafrost groundwater. *Journal of Geophysical Research: Planets*, **115**(E7) (2010).
6. Lasue, J., Clifford, S. M., Conway, S. J., Mangold, N., & Butcher, F. E. The Hydrology of Mars Including a Potential Cryosphere. In Volatiles in the Martian Crust (**pp. 185-246**). *Elsevier* (2019).
7. Orosei R, Lauro, S.E., Pettinelli, E., Cicchetti, A., Coradini, M., Cosciotti, B., Di Paolo, F., Flamini, E., Matteu, E., Pajola, M., Soldovieri, F., Cartacci, M., Cassenti, F., Frigeri, A., Giuppi, S., Martufi, R., Masdea, A., Mitri, G., Nenna, C., Noschese, R., Restano, M., Seu, R. Radar evidence of subglacial liquid water on Mars. *Science* **361**, 490-493 (2018).
8. Lauro, S. E., Soldovieri, F., Orosei, R., Cicchetti, A., Cartacci, M., Mattei, E., ... & Pettinelli, E. Liquid Water Detection under the South Polar Layered Deposits of Mars—A Probabilistic Inversion Approach. *Remote Sensing*, **11**(20), 2445 (2019).
9. Cabrol, N.A., Grin, E.A. Distribution, classification, and ages of Martian impact crater lakes. *Icarus* **142**, 160-172 (1999).
10. Baker, V. R, Water and the Martian landscape. *Nature*, **412**, (6843), 228 (2001).
11. Craddock, R.A., Howard, A.D. The case for rainfall on a warm, wet early Mars. *JGR* **107**(E11), 511, (2002).
12. Pondrelli, M., Rossi, A. P., Marinangeli, L., Hauber, E., Gwinner, K., Baliva, A., & Di Lorenzo, S. Evolution and depositional environments of the Eberswalde fan delta, Mars. *Icarus*, **197**(2), 429-451 (2008).
13. Bibring, J.P., Lamgevin, Y., Mustard, J.F., Poulet, F., Arvidson, R., Gendrin, A., et al. Global mineralogical and aqueous Mars history derived from OMEGA/Mars Express data. *Science* **312**, 400-404 (2006).

14. Ramirez, R., Craddock, R. The geological and climatological case for a warmer and wetter early Mars. *Nature Geoscience* **11**(4), 230-237 (2018).
15. Palumbo, A.M., Head, J.W. Early Mars climate history: Characterizing a "warm and wet" Martian climate with a 3-D global climate model and testing geological predictions. *GRL* **45**, 10249-10258 (2018).
16. Palumbo, A. M., Head, J. W., & Wordsworth, R. D. Late Noachian Icy Highlands climate model: Exploring the possibility of transient melting and fluvial/lacustrine activity through peak annual and seasonal temperatures. *Icarus*, **300**, 261-286 (2018).
17. Laskar J, Correia, A.C.M, Gastineau, M., Joutel, F., Levrard, B., Robutel, P. Long term evolution and chaotic diffusion of the insolation quantities of Mars. *Icarus* **170**, 343-364 (2004).
18. Murray, B. C., Ward, W. R., & Yeung, S. C. Periodic insolation variations on Mars. *Science*, **180**(4086), 638-640 (1973).
19. Ward, W. R. Large-scale variations in the obliquity of Mars. *Science*, **181**(4096), 260-262 (1973).
20. Ward, W. R. Long-term orbital and spin dynamics of Mars (1992).
21. Laskar J., Levrard B., Mustard JF Orbital forcing of the martian polar layered deposits. *Nature* **419**, 375-377, (2002).
22. Laskar J, Correia, A.C.M, Gastineau, M., Joutel, F., Levrard, B., Robutel, P. Long term evolution and chaotic diffucion of the insolation quantities of Mars. *Icarus* **170**, 343-364 (2004).
23. Byrne, S. The polar deposits of Mars. *Annual Review of Earth and Planetary Sciences*, **37**, 535-560 (2009).
24. Guallini, L., Rossi, A.P., Forget, F., Marinangeli, L., Lauro, S.E., Pettinelli, E., Seu, R., Thomas, N. Regional stratigraphy of the south polar layered deposits (Promethei Lingula, Mars): "Discontinuity-bounded" units in images and radargrams. *Icarus* **308**, 76-107 (2018).
25. Smith, I. B., Diniega, S., Beaty, D. W., Thorsteinsson, T., Becerra, P., Bramson, A. M., ... & Spiga, A. 6th international conference on Mars polar science and exploration: Conference summary and five top questions. *Icarus*, **308**, 2-14. (2018).
26. Head, J.W., Pratt, S. Extensive Hesperian-aged south polar ice sheet on Mars: Evidence for massive melting and retreat, and lateral flow and ponding of meltwater. *JGR* **106**(E6), 12275-12299 (2001).
27. Fastook, J.L., Head, J.W., Marchant, D.R., Forget F., Madeleine, J-B. Early Mars climate near the Noachian-Hesperian boundary: Independent evidence for cold conditions form basal melting of the south polar ice sheet (Dorsa Argentea Formation) and implications for valley network formation. *Icarus* **219**, 25-40 (2012).

28. Grott, M., Baratoux, D., Hauber, E., Sautter, V., Mustard J., Gasnault, O., Ruff, S.W., Karato, S-I, Debaille, V., Knapmeyer, M., Sohl, F., Van Hoolst, T., Breuer, D., Morschhauser, A., Toplis, M.J. Long-term evolution of the Martian crust-mantle system. *Space Sci Rev* **174**, 49-111 (2013).
29. Grima, C., Costard, F., Kofman, W., Saint-Bezar, B., Servain, A., Remy, F., Mouginot, J., Herique, A., Seu, R. Large asymmetric polar scarps on Planum Australia, Mars: Characterization and evolution. *Icarus* **212**, 96-109 (2011).
30. Guallini, L., Brozzetti, F., Marinangeli, L. Large-scale deformational systems in the South Polar Layered Deposits (Promethei Lingula, Mars): "Soft-sediment" and deep-seated gravitational slope deformations mechanisms. *Icarus* **220**, 821-843 (2012).
31. Guallini, L., Rossi, A. P., Lauro, S. E., Marinangeli, L., Pettinelli, E., & Seu, R. "Unconformity-Bounded" Stratigraphic Units in the South Polar Layered Deposits (Promethei Lingula, Mars). In STRATI 2013 (pp. 331-335). *Springer, Cham*. (2014).
32. Wieczorek, M.A. Constraints on the composition of the martian south polar cap from gravity and topography. *Icarus* **196**, 506-517 (2008).
33. Fisher, D.A., Hecht, M.H., Kounaves, S.P., Catling, D.C. A perchlorate brine lubricated deformable bed facilitating flow on the north polar cap of Mars: Possible mechanism for water table recharging. *JGR* **115**, E00E12 (2010).
34. Sori, M.M., Bramson, A.M. Water on Mars, with a grain of salt: Local heat anomalies are required for basal melting of ice at the South Pole today. *GRL* **46**, 10.1029/2018GL080985 (2019).
35. Hamilton, C.W., Fagents, S.A., Wilson, L. Explosive lava-water interactions in Elysium Planitia, Mars: Geologic and thermodynamic constraints on the formation of the Tartarus Colles cone groups. *JGR* **115**, E09006 (2010).
36. Horvath, D.G., Andrews-Hanna, J.C. The thickness and morphology of a young pyroclastic deposit in Cerberus Palus, Mars: Implications for the formation sequence. *LPSC* **49**, abstr # 2435 (2018).
37. Souček, O., Bourgeois, O., Pochat, S., Guidat, T. A 3 Ga old polythermal ice sheet in Isidis Planitia, Mars: dynamics and thermal regime inferred from numerical modeling. *EPSL* **426**, 176-190 (2015).
38. Bell R.E, Studinger, M., Fahnestock, M.A, Shuman, C.A. Tectonically controlled subglacial lakes on the flanks of the Gamburtsev Subglacial Mountains, East Antarctica. *Geophys Res Lett* **33**, L02504 (2006).
39. Diez, A., Matsuoka, K., Jordan, T.A., Kohler, J., Ferraccioli, F., Corr, H.F., Olesen, A.V., Forsberg, R., Casal, T.G. Patchy lakes and topographic origin for fast flow in the Recovery Glacier System, East Antarctica. *J Geophys Res Earth Surface* **124**, (2019).

40. Plaut, J. J., Picardi, G., Safaeinili, A., Ivanov, A. B., Milkovich, S. M., Cicchetti, A., ... & Clifford, S. M. Subsurface radar sounding of the south polar layered deposits of Mars. *Science*, **316**(5821), 92-95 (2007).
41. Bogorodskii, V., Bentli, C., & Gudmandsen, P. (1983). Radio glaciology. Leningrad Gidrometeoizdat.
42. Carter, S. P., Blankenship, D. D., Peters, M. E., Young, D. A., Holt, J. W., & Morse, D. L. Radar-based subglacial lake classification in Antarctica. *Geochemistry, Geophysics, Geosystems*, **8**(3) (2007).
43. Peters, M. E., Blankenship, D. D., & Morse, D. L. Analysis techniques for coherent airborne radar sounding: Application to West Antarctic ice streams. *Journal of Geophysical Research: Solid Earth*, **110**(B6) (2005).
44. Young, D. A., Schroeder, D. M., Blankenship, D. D., Kempf, S. D., & Quartini, E. The distribution of basal water between Antarctic subglacial lakes from radar sounding. *Philosophical Transactions of the Royal Society A: Mathematical, Physical and Engineering Sciences*, **374**(2059), 20140297 (2016).
45. Schroeder, D. M., Blankenship, D. D., & Young, D. A. Evidence for a water system transition beneath Thwaites Glacier, West Antarctica. *Proceedings of the National Academy of Sciences*, **110**(30), 12225-12228 (2013).
46. Schroeder, D. M., Blankenship, D. D., Raney, R. K., & Grima, C. Estimating subglacial water geometry using radar bed echo specularity: application to Thwaites Glacier, West Antarctica. *IEEE Geoscience and Remote Sensing Letters*, **12**(3), 443-447 (2014).
47. Palmer S. J., Dowdeswell J. A., Christoffersen P., Young D. A., Blankenship D. D., Greenbaum J. S., ... & Siegert M. J. Greenland subglacial lakes detected by radar. *Geophysical Research Letters*, **40**(23), 6154-6159 (2013).
48. Oswald, G. K. A., & Gogineni, S. P. Recovery of subglacial water extent from Greenland radar survey data. *Journal of Glaciology*, **54**(184), 94-106 (2008).
49. Oswald, G. K., & Gogineni, S. P. Mapping basal melt under the northern Greenland Ice Sheet. *IEEE Transactions on Geoscience and Remote Sensing*, **50**(2), 585-592 (2011).
50. Jordan, T. M., Bamber, J. L., Williams, C. N., Paden, J. D., Siegert, M. J., Huybrechts, P., ... & Gillet-Chaulet, F. An ice-sheet-wide framework for englacial attenuation from ice-penetrating radar data *The Cryosphere*, Copernicus, **10**, pp.1547 - 1570 (2016).
51. Jordan, T. M., Cooper, M. A., Schroeder, D. M., Williams, C. N., Paden, J. D., Siegert, M. J., & Bamber, J. L. Self-affine subglacial roughness: Consequences for radar scattering and basal water discrimination in northern Greenland. *The Cryosphere*, **11**(3), 1247 (2017).

52. Oswald, G. K., Rezvanbehbahani, S., & Stearns, L. A. Radar evidence of ponded subglacial water in Greenland. *Journal of Glaciology*, **64**(247), 711-729 (2018).
53. Jordan, T. M., Williams, C. N., Schroeder, D. M., Martos, Y. M., Cooper, M. A., Siegert, M. J., Paden, J. D., Huybrechts, P., and Bamber, J. L.: A constraint upon the basal water distribution and thermal state of the Greenland Ice Sheet from radar bed echoes, *The Cryosphere*, **12**, 2831-2854, (2018).
54. Bowling, J. S., Livingstone, S. J., Sole, A. J., & Chu, W. Distribution and dynamics of Greenland subglacial lakes. *Nature Communications*, **10**(1), 2810 (2019).
55. Rutishauer, A., Blankenship, D.D., Sharp, M., Skidmore, M.L., Greenbaum, J.S., Grima, C., Schroeder, D.M., Dowdeswell, J.A., Young, D.A. Discovery of a hypersaline subglacial lake complex beneath Devon Ice Cap, Canadian Arctic. *Sci Adv* **4**, eaar4353 (2018).
56. Lauro, S. E., Mattei, E., Pettinelli, E., Soldovieri, F., Orosei, R., Cartacci, M., ... & Giuppi, S. Permittivity estimation of layers beneath the northern polar layered deposits, Mars. *Geophysical Research Letters*, **37**(14) (2010).
57. Dowdeswell, J. A., & Siegert, M. J. The physiography of modern Antarctic subglacial lakes. *Global and Planetary Change*, **35**(3-4), 221-236 (2003).
58. Fricker, H.A., Siegfried, M.R., Carter, S.P. Scambos, T.A. A decade of progress in observing and modelling Antarctic subglacial water systems. *Phil Trans R Soc A* **374**: 20140294 (2015).
59. Duxbury, N. S., Zotikov, I. A., Nealson, K. H., Romanovsky, V. E., & Carsey, F. D. A numerical model for an alternative origin of Lake Vostok and its exobiological implications for Mars. *Journal of Geophysical Research: Planets*, **106**(E1), 1453-1462 (2001).
60. Gilichinsky, D., Rivkina, E., Shcherbakova, V., Laurinavichuis, K., & Tiedje, J. Supercooled water brines within permafrost—an unknown ecological niche for microorganisms: a model for astrobiology. *Astrobiology*, **3**(2), 331-341 (2003).
61. Mikucki, J. A., Auken, E., Tulaczyk, S., Virginia, R. A., Schamper, C., Sørensen, K. I., ... & Foley, N. Deep groundwater and potential subsurface habitats beneath an Antarctic dry valley. *Nature communications*, **6**, 6831 (2015).
62. Siegert, M.J. Antarctic subglacial lakes. *Earth-Sci Rev* **50**, 29-50 (2000).
63. Dugan, H.A., Doran, P.T. Tulaczyk, S., Mikucki, J.A., Arcone, S.A., Auken, E., Schamper, C., Virginia, R.A. Subsurface imaging reveals a confined aquifer beneath an ice-sealed Antarctic lake. *GRL* **42**, 96-103 (2015).
64. Goeller, S., Steinhage, D., Thoma, M., Grosfeld. Assessing the subglacial lake coverage of Antarctica. *Annals of Glaciology* **57**. (2016).

65. Studinger, M., Bell, R.E., Karner, G.D., Tikku, A.A., Holt, J.W., Morese, D.L., Richter, T.G., Kempf, S.D., Peters, M.E., Blankenship, D.D., Sweeney, R.E., Rystrom, V.L. Ice cover, landscape setting, and geological framework of Lake Vostok, East Antarctica. *EPSL* **205**, 195-210 (2003).
66. Schroeder, D.M., Blankenship, D.D., Young, D.A., Quartini, E. Evidence for elevated and spatially variable geothermal flux beneath the West Antarctic ice sheet. *PNAS* **111**(25) (2014).
67. Siegert, M.J., Ross, N., Corr, H., Smith, B., Jordan, T., Bingham, R.G., Ferraccioli, F., Rippin, D.M., Le Brocq A Boundary conditions of an active West Antarctic subglacial lake: implications for storage of water beneath the ice sheet. *The Cryosphere* **8**, 15-24 (2014).
68. Carter, S. P., Fricker, H. A., & Siegfried, M. R. Antarctic subglacial lakes drain through sediment-floored canals: theory and model testing on real and idealized domains. *The Cryosphere*, **11**(1), 381 (2017).
69. Bell, R.E, Studinger M, Tikku, A.A, Clarke, G.K.C, Gutner, M.M, Meertens, C. Origin and fate of Lake Vostok water frozen to the base of the East Antarctic ice sheet. *Nature* **416**, 307-310 (2002).
70. Hubbard, A., Lawson, W., Anderson, B., Hubbard, B., & Blatter, H. Evidence for subglacial ponding across Taylor Glacier, Dry Valleys, Antarctica. *Annals of Glaciology*, **39**, 79-84 (2004).
71. Brass, G. W. Stability of brines on Mars. Icarus, **42**(1), 20-28 (1980).
72. Ojha, L, Wilhelm, M.B., Murchie, S.L., McEwen, A.S., Wray, J.J. Spectral evidence for hydrated salts in recurring slope lineae on Mars. *Nature Geoscience* **8**, 829-832 (2015).
73. Rennó, N. O., Bos, B. J., Catling, D., Clark, B. C., Drube, L., Fisher, D., ... & Kounaves, S. P. Possible physical and thermodynamical evidence for liquid water at the Phoenix landing site. *Journal of Geophysical Research: Planets*, **114**(E1) (2009).
74. Hecht, M.H., Kounaves, S.P., Quinn, R.C., West, S.J., Young, S.M.M., Ming, DW, Catling, D.C., Clark, B.C., Boynton, W.V., Hoffman, J., DeFlores, L.P., Gospodinova, K., Kapit, J., Smith, P.H. Detection of perchlorate and soluble chemistry of Martian soil at the Phoenix Lander Site. *Science* **325**, 64-67 (2009).
75. Osterloo, M. M., Anderson, F. S., Hamilton, V. E., & Hynek, B. M. Geologic context of proposed chloride-bearing materials on Mars. *Journal of Geophysical Research: Planets*, **115**(E10) (2010).
76. Hanley, J., Chevrier, V.F., Berget, D.J., Adams, R.D. Chlorate salts and solutions on Mars. *GRL* **39**, L08201, (2012).
77. Glavin, D.P., Freissinet, C., Miller, K.E., Eigenbrode, J.L., Brunner, A.E., Buch, A., Sutter, B., Archer, P.D., Atreya, S.K., Brinckerhoff, W.B., Cabane, M., Coll, P., Conrad, P.G., Coscia, D., Dworkin, J.P., Franz, H.B., Grotzinger, J.P., Leshin, L.A., Martin, M.G., McKay, C., Ming, D.W.,

Navarro-Gonzáles, R., Pavlov, A., Steele, A., Summons, R.E., Szopa, C., Teinturier, S., Mahaffy, P.R. Evidence for perchlorates and the origin of chlorinated hydrocarbons detected by SAM at the Rocknest Aeolian deposit in Gale Crater. *JGR Planets* **118**, 1955-1973 (2013).

78. Zorzano, M. P., Mateo-Martí, E., Prieto-Ballesteros, O., Osuna, S., & Renno, N. Stability of liquid saline water on present day Mars. *Geophysical Research Letters*, **36**(20) (2009).
79. Gough, R. V., Chevrier, V. F., & Tolbert, M. A. (2014). Formation of aqueous solutions on Mars via deliquescence of chloride–perchlorate binary mixtures. Earth and Planetary Science Letters, 393, 73-82.
80. Gough RV, Chevrier VF, Tolbert MA (2016) Formation of liquid water at low temperatures via the deliquescence of calcium chloride: Implications for Antarctica and Mars. PSS 131, 79-87.
81. Gough, R. V., Chevrier, V. F., Baustian, K. J., Wise, M. E., & Tolbert, M. A. Laboratory studies of perchlorate phase transitions: Support for metastable aqueous perchlorate solutions on Mars. *Earth and Planetary Science Letters*, **312**(3-4), 371-377 (2011).
82. Primm, K. M., Gough, R. V., Chevrier, V. F., & Tolbert, M. A. Freezing of perchlorate and chloride brines under Mars-relevant conditions. *Geochimica et Cosmochimica Acta*, **212**, 211-220 (2017).
83. Primm, K. M., Stillman, D. E., & Michaels, T. I. Investigating the hysteretic behavior of Mars-relevant chlorides. *Icarus* (2019).
84. Toner, J.D., Catling, D.C. Chlorate brines on Mars: Implications for the occurrence of liquid water and deliquescence. *EPSL* **497**, 161-168 (2018).
85. Pestova, O. N., Myund, L. A., Khripun, M. K., & Prigaro, A. V. Polythermal study of the systemsM(ClO4)2–H2O (M2+=Mg2+, Ca2+, Sr2+, Ba2+). *Russian Journal of Applied C*hemistry, **78**(3), 409–413 (2005).
86. Chevrier, V. F., Hanley, J., & Altheide, T. S. Stability of perchlorate hydrates and their liquid solutions at the Phoenix landing site, Mars. *Geophysical Research Letters*, **36**, L10202 (2009).
87. Toner, J.D., Catling, D.C., Light, B. The formation of supercooled brines, viscous liquids, and low-temperature perchlorate glasses in aqueous solutions relevant to Mars. *Icarus* **233**, 36-47 (2014).
88. Maus, D., Heinz, J., Schirmack, J., Airo, A., Kounaves, S. P., Wagner, D., & Schulze-Makuch, D., Methanogenic Archaea Can Produce Methane in Deliquescence-Driven Mars Analog Environments. *Scientific Reports*, **10**(1), 1-7 (2020).
89. Stamenković, V., Ward, L. M., Mischna, M., & Fischer, W. W., O 2 solubility in Martian near-surface environments and implications for aerobic life. *Nature Geoscience*, **11**(12), 905 (2018).

90. Jordan, R., et al., The Mars express MARSIS sounder instrument. Planetary and Space *Science*, **57**(14-15), 1975-1986 (2009).
91. Cicchetti A., et al., Observations of Phobos by the Mars Express radar MARSIS: Description of the detection techniques and preliminary results. *Adv. Space Res*.,**60**, 2289-2302 (2017).
92. Berry, M. V. The statistical properties of echoes diffracted from rough surfaces. *Philosophical Transactions of the Royal Society of London*. Series A, Mathematical and Physical Sciences, **273**, (1237), 611-654 (1973).
93. Cuffey, K. M., & Paterson, W. S. B. *The physics of glaciers*. Academic Press. (2010).
94. Li, J., Andrews-Hanna, J. C., Sun, Y., Phillips, R. J., Plaut, J. J., & Zuber, M. T. Density variations within the south polar layered deposits of Mars. *Journal of Geophysical Research: Planets*, ***117***(E4) (2012).
95. Taylor, J. Introduction to error analysis, the study of uncertainties in physical measurements (1997).
96. Tarantola, A., Inverse problem theory and methods for model parameter estimation. *Siam*., **89** (2005).
97. Mouginot, J., Kofman, W., Safaeinili, A., Grima, C., Hérique, A., & Plaut, J. J. MARSIS surface reflectivity of the south residual cap of Mars. *Icarus*, **201**(2), 454-459(2009).
98. Lauro, S. E., Mattei, E., Soldovieri, F., Pettinelli, E., Orosei, R., & Vannaroni, G. Dielectric constant estimation of the uppermost Basal Unit layer in the martian Boreales Scopuli region. *Icarus*, **219**(1), 458-467 (2012).

Methods

MARSIS data. MARSIS radar is a nadir-looking pulse limited radar sounder that can operate in two main observational modalities: Sub-Surface (SS) Mode and Active Ionosphere Sounding (AIS) Mode. In SS mode, MARSIS transmits a 250 µs chirp with a 1MHz bandwidth. According to the predicted Solar Zenith Angle (SZA), the chirp central frequency is selected among 4 different values (1.8, 3, 4 and 5 MHz) to work well above the cut-off plasma frequency of the Martian ionosphere[90]. After range compression and Hanning windowing, the achievable range resolution in pure ice is about 55 m (assuming a velocity of 170 m/µs). In this work, we only analyzed unprocessed data to avoid the uncertainty due to the incoherent integration performed on- board in normal mode[7]. Two alternative data acquisition methods were used[91]: i) the Flash Memory (FM) technique, which collects discontinuous intervals of unprocessed/raw data along orbits; and ii) the Superframe acquisition mode, which continuously collects data but along shorter orbits (Fig.1).

MARSIS data were collected in different years (2010 – 2019) and during different Martian seasons, therefore each orbit refers to particular conditions of the Martian ionosphere. Because the ionosphere can cause dispersion on the transmitted signal, reducing the echo intensity and producing a broadening of the received signal, we normalized all quantities (i.e., surface and basal intensity and acuity) to the median of the relevant surface quantity along each orbit. In particular, the use of the median minimizes the effects caused by local surface echo power fluctuations, which are sometimes observed in the data, without altering the along track variation of the basal reflectivity and acuity.

In this work we present and discuss only the data collected at 4MHz, as it is the largest and most robust dataset. The data collected at the other frequencies are sparser (especially the 3MHz that is also more affected by the ionosphere) and thus less statistically significant (Supplementary Fig.1). Despite this fact, the analysis of such data supports the results obtained at 4MHz.

Spatial smoothing and acuity. We processed MARSIS data according to the method developed by Oswald and Gogineni[48], which applies an along-track average to the radar traces (spatial smoothing) in order to reduce the power variance due to variable roughness[92,43]. In our analysis, the along-track waveform averaging window W is set equal to the diameter of the pulse-limited footprint area:

$$W = 2\sqrt{c\frac{p}{2}\left(H+\frac{z}{n}\right)} \cong 2\sqrt{c\frac{p}{2}H}, \qquad (1)$$

where $p = 1\mu s$ is the transmitted pulse length, H is the spacecraft altitude (this quantity can vary between 250 and 900 km), c is velocity of light in a vacuum, z is the depth of the reflector and $n \cong$

1.71 is the water ice refractive index. For example, considering a spacecraft height $H = 400$km the resulting window is $W \cong 15km$.

In addition, we computed the acuity A_c, which is an indication of interface roughness, from the depth aggregated echo power[52] as follows:

$$A_c = \frac{max\{x_r^2(t)\}}{\sum_{t=\tau-T/2}^{\tau+T/2} x_r^2(t)}, \qquad (2)$$

where $x_r(t)$ is the received pulse generated by a reflector located at a time delay τ (e.g., surface or bedrock), $T = \sqrt{\frac{H}{2\nu c}}$ (ν is the operating frequency).

Basal topography and hydraulic potential. We computed the basal topography (B) and the hydraulic potential (ϕ_H) along the observations reported in Fig.3 according to the following equations[93]:

$$B = S - h \qquad (3)$$

and

$$\phi_H = \rho_w g_M (S - h(1 - \rho_{ice}/\rho_w)) \qquad (4)$$

Where S is the surface topography (based on MOLA data), h is the SPLDs thickness computed assuming a permittivity $\varepsilon_{ice} = 3.4$, $\rho_w = 1980\ \mathrm{kg/m^3}$is the density of the perchlorate solution[33], $\rho_{ice} = 1100\ \mathrm{kg/m^3}$ the average density of the SPLDs[94] and $g_M = 3.72\ m/s^2$ is the Martian gravity (Supplementary Fig.2). The uncertainties Δu associated with these parameters (where $u = B$ or $u = \phi_H$, depending on the used equation) have been computed applying the statistical propagation formula[95], under the assumption that all uncertainties are independent and uncorrelated:

$$\Delta u = \sqrt{\sum_i \left(\frac{\partial u}{\partial x_i} \Delta x_i\right)^2} \qquad (5)$$

where x_i are the variables (e.g. $S, h, \ldots$) in equations 3 and 4 and Δx_i the associated uncertainties. In Eq. (5) $\Delta h = 61m$, $\Delta S = 61m$ and $\Delta\rho_{ice} = 115\ kg/m^3$. Note that we have neglected the uncertainties related to the density of perchlorate brines and Martian gravity.

Bed-echo intensity variability. We used the intensity variability parameter σ_I to localize the transition between dry (or frozen) and wet bed conditions[53]. The parameter σ_I is given by:

$$\sigma_I = \Delta R\sqrt{f^2(1-f) + (1-f)^2 f} \qquad (6)$$

where

$$\Delta R = 20log_{10}\left(\left|\frac{\sqrt{\varepsilon_b}-\sqrt{\varepsilon_{ice}}}{\sqrt{\varepsilon_b}+\sqrt{\varepsilon_{ice}}}\right|\left|\frac{\sqrt{\varepsilon_{dry}}+\sqrt{\varepsilon_{ice}}}{\sqrt{\varepsilon_{dry}}-\sqrt{\varepsilon_{ice}}}\right|\right) \qquad (7)$$

With ε_b the dielectric permittivity of the basal material, ε_{ice} the permittivity of the SPLDs and ε_{dry} the permittivity of the dry rock. In addition, f is the fraction of wet area (wet–dry mixing ratio in Jordan et al. [53]) inside the radar footprint. Supplementary Fig.3 illustrates the intensity variability as a function of the basal permittivity for two values of the mixing ratio f.

We computed the intensity variability σ_I (expressed in dB) along each orbit at x_i position, as follows:

$$\sigma_I(x_i) = \frac{10}{\ln(10)}\frac{\sqrt{\frac{1}{N}\sum_{x=x_i-W/2}^{x_i+W/2}\left[P_{ag}(x)-<P_{ag}(x_i)>\right]^2}}{<P_{ag}(x_i)>} \qquad (8)$$

where $P_{ag}(x)$ is the aggregated power computed according to Jordan et al. [53], and $< P_{ag}(x_i) >$ is the average echo power:

$$< P_{ag}(x_i) >= \frac{1}{N}\sum_{x=x_i-W/2}^{x_i+W/2} P_{ag}(x) \qquad (9)$$

The observations collected around the bright area show specific values of the bed-echo intensity variability. In particular, the radar observations crossing approximately the center of the main body of liquid water (Fig.3 and Supplementary Fig.4 and Fig.5) exhibit an intensity variability exceeding the fairly conservative threshold of 6dB[53] and therefore clearly indicate a transition from dry to wet basal material. On the other hand, the observations passing on the edge of the main body or on the other patches, even if still showing an abrupt change in intensity variability, do not exceed 4-5dB. These results can be explained considering the intersection between the radar footprint and the bed conditions (dry/wet), which is accounted for by the parameter f (Supplementary Fig.3, Fig.4 and Fig.5).

Permittivity map.

The basal permittivity map was generated applying an inversion probabilistic approach[96] to the intensity values collected along the radar profiles shown in Fig. 1b. The procedure and the parameters used are reported in Lauro et al.[8].

As a first step, to generate the map reported in Fig.5, we applied a mesh refinement technique to obtain pixels containing about 100 samples. All pixels having fewer samples were discarded. For each pixel, we computed a probability density function of the basal permittivity and we assigned the median value of such distribution to the pixel coordinates in the scatter map (Supplementary Fig. 6). Our analysis was focused on the area having the highest pixel density (white dashed box in Supplementary Fig. 6) which was interpolated to generate a contour map (Fig. 5). Nevertheless, the areas with lower pixel densities (outside the white dashed box) are very consistent (spatial continuity) and characterized by low permittivity values (dry rocks) except for a small area in the North-East, where the permittivity values are higher. This latter area was not included in the analysis given the low MARSIS coverage and the lack of crossing orbits.

Note that, in the inversion procedure, both surface and basal roughness were not accounted for. In the area, the surface is very smooth at the MARSIS scale[97] whereas the basal roughness is not well constrained. Therefore, the basal permittivity (Fig.5) computed with the inversion could be, in principle, underestimated[98]. However, this is not the case for the main body of liquid water as the subsurface and surface acuity values are similar (Fig.3b). The acuity values measured on the other patches of water are only slightly lower, suggesting that, if present, the underestimation of the permittivity should not be very large.

Supplementary information

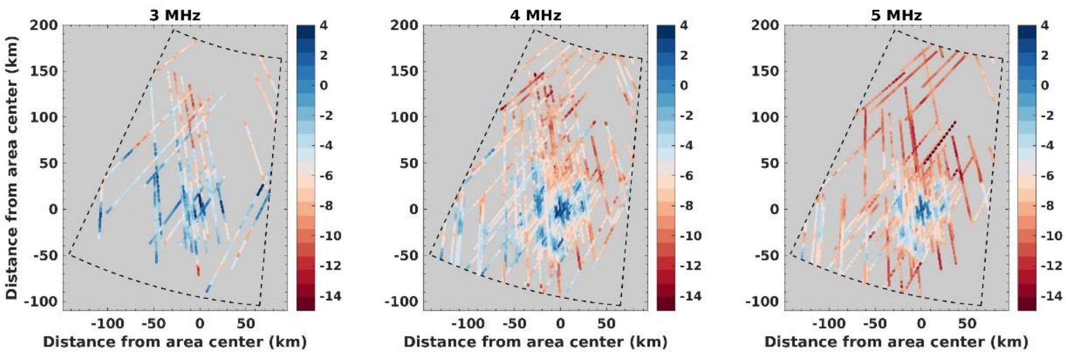

Supplementary Fig.1 Normalized basal reflectivity maps of the observations collected in the investigated area (185-205E and 79.5-84.1S) at 3, 4 and 5MHz.

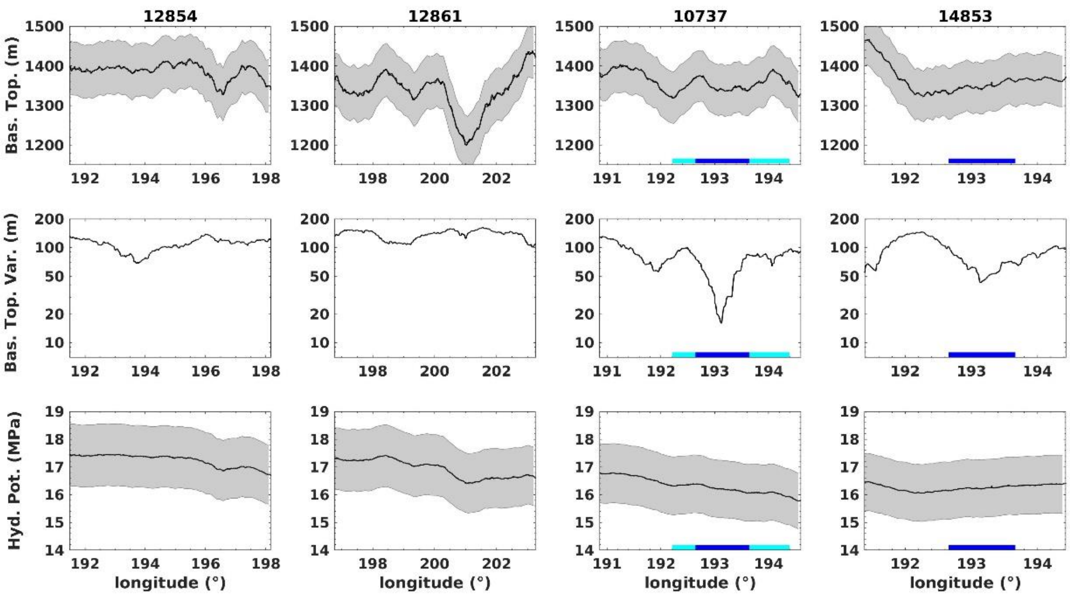

Supplementary Fig.2 Top row indicates the basal topography with the associated uncertainty (gray band). The central row represents the basal topography variability, computed applying a moving average window (Eq.1), which shows local minima in correspondence to the main body of water (dark blue lines). Bottom row represents the hydraulic potential with relevant uncertainty (gray band). The first two columns refer to the observations collected outside the bright area and the last two those collected inside the bright area. Dark blue lines indicate the position of the main body of liquid water, cyan lines the lateral water patches. In the wet areas the along-track variations of basal topography and hydraulic potential are of the same order of magnitude as the uncertainties, indicating that MARSIS does not have the sensitivity to measure such variations.

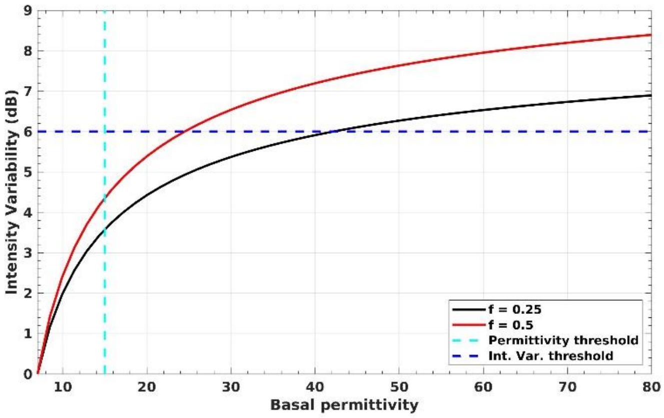

Supplementary Fig. 3 Intensity variability computed using equations 3 and 4, assuming $\varepsilon_{dry} = 7$ and considering two different wet-dry mixing ratios (black and red lines). The cyan dashed line represents the permittivity threshold $\varepsilon_b = 15$ which, on Earth, is usually associated with wet materials[7] and the dashed blue line is the intensity variability threshold for dry to wet basal transition[53].

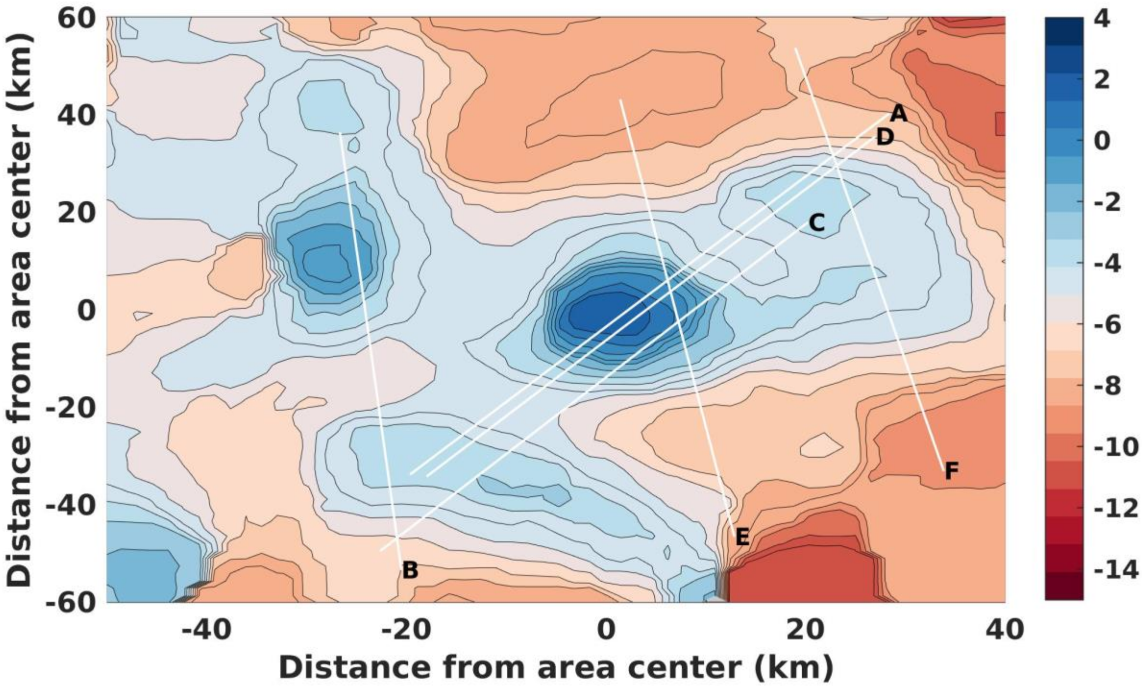

Supplementary Fig.4 Enlargement of the normalized basal intensity map shown in Fig.4a. White lines highlight six observations crossing the main body of water and the lateral patches.

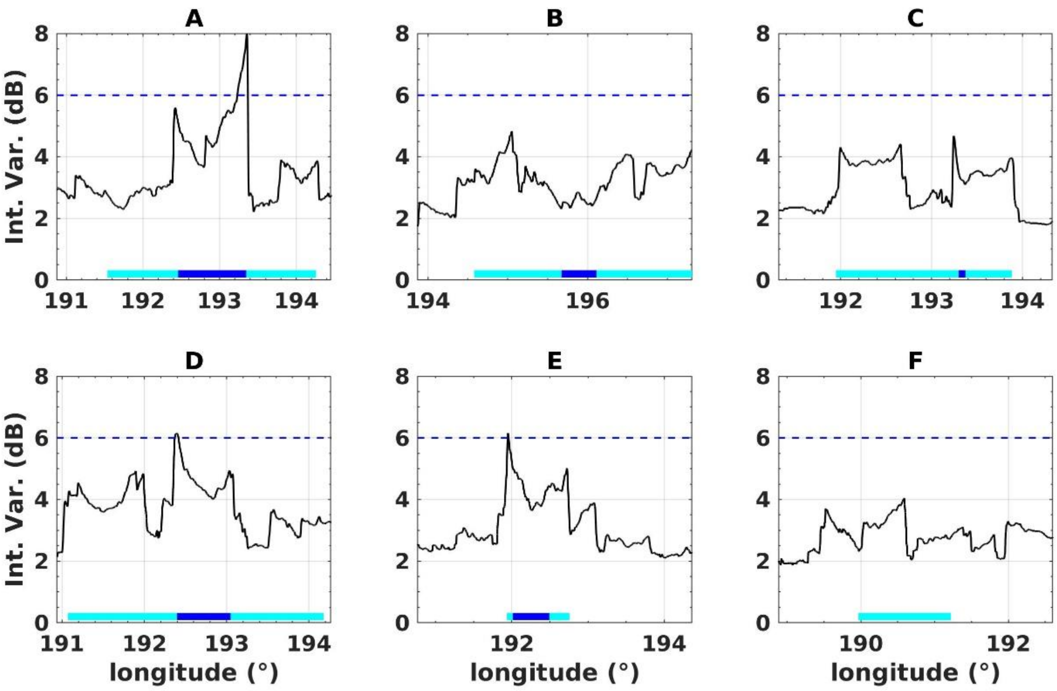

Supplementary Fig.5 Intensity variability values computed using equation 3 for the six observations illustrated in Supplementary Fig. 4. The blue dashed lines mark the intensity variability threshold for the dry-wet transition according to Jordan et al.[53]. Dark blue lines indicate the position of the main body of liquid water, cyan lines the lateral water patches.

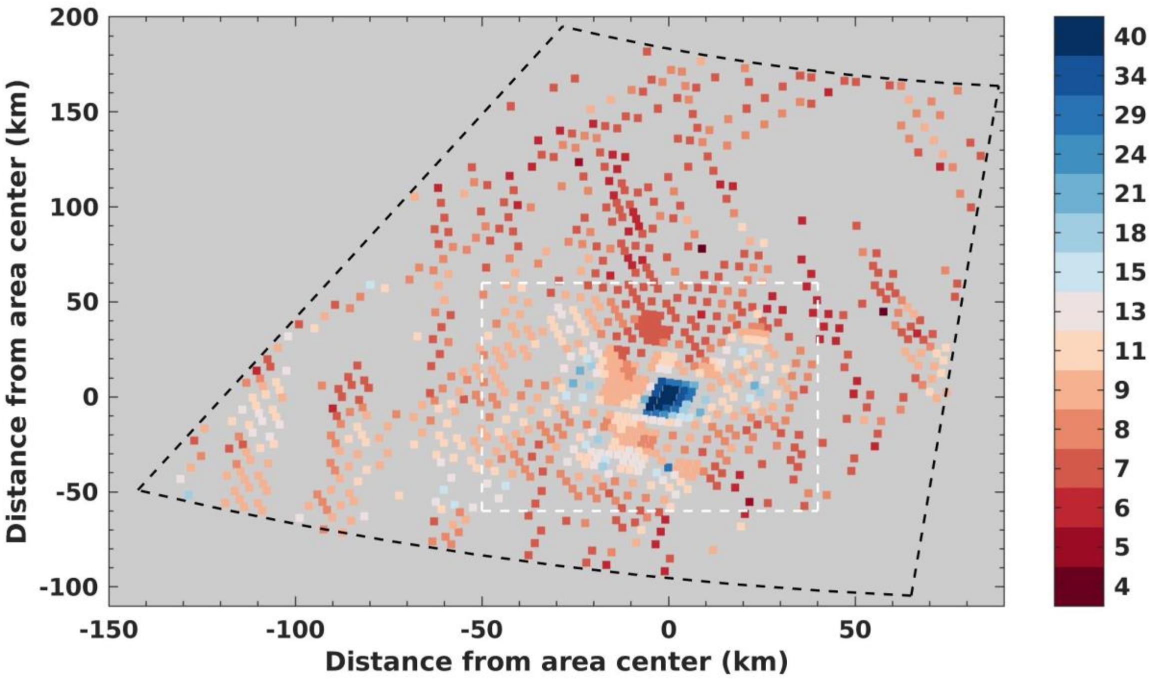

Supplementary Fig. 6 Scatter map of the basal permittivity. The white dashed box indicates the area analyzed in Fig. 5. The size of the dots in the map is not representative of the pixel dimension.